ARCHIVES OF MECHANICS
Arch. Mech. **71** (2), 95–111, 2019, DOI: 10.24423/aom.3091

Stability of feed forward artificial neural networks versus nonlinear structural models in high speed deformations: A critical comparison

M. STOFFEL, F. BAMER, B. MARKERT

Institute of General Mechanics, RWTH Aachen University, Templergraben 64, D-52056 Aachen, Germany, e-mail: stoffel@iam.rwth-aachen.de

In recent years, artificial neural networks have been proposed for engineering applications, such as predicting stresses and strains in structural elements. However, the question arises, how many complex influences can be included in an artificial neural network (ANN) and how accurate these predictions are in comparison to classical finite element solutions. A weakness of finite element predictions is that they can behave sensitive and unstable to changes in material parameters. An ANN does not need an underlying model with parameters and uses input variables, only. In the present study the stability of numerical results obtained by ANN and FEM are compared to each other for a problem in structural dynamics. The result gives new insight about the possibilities to predict accurately structural deformations by means of ANNs. As an example for highly complex geometrically and physically nonlinear structural deformations, the response of circular metal plates subjected to shock waves is investigated.

Key words: artificial neural network, structural mechanics, shock-wave loaded structures, viscoplasticity, shell theory.

1. Introduction

The present study focuses on predictions of structural behaviour by means of ANNs, taking the sensitivity with respect to changes in input variables into account. In literature, ANNs for engineering applications were proposed for stress-strain curves in [1] at high temperatures. For the design of structures, artificial intelligence was applied on steel materials also in the nonlinear range [2]. In manufacturing processes and reliability studies of structures, the application of an ANN was proposed in [3, 4] and influences of parameters in final results were discussed. Even for nuclear reactors an ANN is proposed for the embrittlement of steel pressure vessels [5]. The purpose of the development of an ANN can be to replace a continuum mechanical model completely. The ANN must be trained by any data in order to adapt it to the particular application [6]. For this reason, one method, reported in literature, is to train an ANN by measurements only and to create in this way a numerical code, based on examples and experience [1, 7, 8]. This motivation is supported by the fact, that an ANN is theoretically able to approximate any arbitrary function [9]. However, the approach to determine a function by means of ANNs can be mathematically nonconstructive, leading to the problem, that internal variables of the ANN, e.g the number of hidden layers, have to be proposed by the user. In the same way the number of weights between the layers and biases are concerned [8, 10] and have to be defined by an iterative process, based on an optimum criterion, e.g. the least-square method. If the ANN is finally trained by experimental data, it can very precisely recalculate the measured output values. However, it is documented in literature that even well-trained ANNs can cause inaccurate results, if the input data differs from the trained set of values, [11, 12, 13]. For this reason, the aim of the present study is to investigate the stability of ANN predictions, if changes in input parameters occur. This problem can be caused by scattering of measurements and are intensified, if complex short time processes are concerned. Here, complex nonlinear structural deformations under high strain rates after shock-wave loading are studied. All experiments were carried out in a shock tube, where fast plate deflections and pressure changes were recorded by means of short-time measurement techniques. In order to predict these structural deformations by means of a classical FEM approach in a previous work [14], it was necessary to use a geometrically nonlinear structural model taking first-order shear deformations into account. After an enhancement of this shell model with viscoplastic theories, a finite element code was adopted, which was able to predict the plate specimens behaviour. Research on the structural response including viscoplastic material behaviour is still of current interest, e.g. [15, 16]. However, the effort to identify material parameters can be circumstantial and can lead to scattering of parameters. In contrast to the FEM, an ANN generates synapse matrices, including weights of given input neurons, leading to an algebraic system of equations with components, which can hardly be interpreted, see [17, 18]. This effect remains the same, independently if the ANN replaces an entire structure or only a material law as it is done e.g. with neural network constitutive equations [17, 19, 20]. However, due to the reduction of a complicated structural or material model to synapse matrix multiplication with an ANN, the advantage of an ANN can be the rapid calculation of a complex boundary value problem in comparison to a finite element simulation. In the present study, an additional advantage is investigated, namely the stability of the trained network, if changes in input neurons occur. This leads to a new perception of the use of trained ANNs. Instead of using already trained neural networks for predicting new output signals with changed input data, the study will show the stability of an ANN even if input parameters change. Here, ANNs with various hidden layers are proposed, trained with experimental data, and, finally, the accuracy of the trained network is investigated by additional experiments. The study deals with metal structures subjected to impulsive loadings in a shock tube. Networks with more than one hidden layer can be regarded in literature [21] as a step towards deep learning. The already trained network is fed with additional input data, which varies from the measurements used for training. Differences in output results are a criterion for the accuracy of the ANN. Regardless of the complexity of the in-house experiments, the sample rate used in the measurements is sufficient for the required number of data points to feed an ANN. Simultaneously, finite element simulations of the structural deformations are carried out with variations in material parameters leading to changes in numerical results. Due to the fact, that material parameters do not occur in the ANN, its sensitivity is studied with respect to variations in input data.

2. Experiment

In order to train the neural network, experiments with a shock tube are conducted, see Fig. 1. Based on experiences from former studies [14], measurements of structural deformations and pressures during shock wave loadings are carried out. Here, circular metal plates with 138 mm diameter and 2 mm thickness are used. In the present study, steel plates were subjected to shock waves, however, it is possible to insert aluminum and copper plates as well. The pressure load is caused by separating two chambers, high (HPC) and low (LPC) pressure chamber, with different pressures and gases from each other by a membrane. If the membrane bursts, then a shock wave is striking the plate specimen at the end of the LPC leading to elastic-viscoplastic deformations of the plate specimen. By means of short time measurement techniques, the pressure acting on the plate and the mid-point displacement of the plate are measured during the impulse duration.

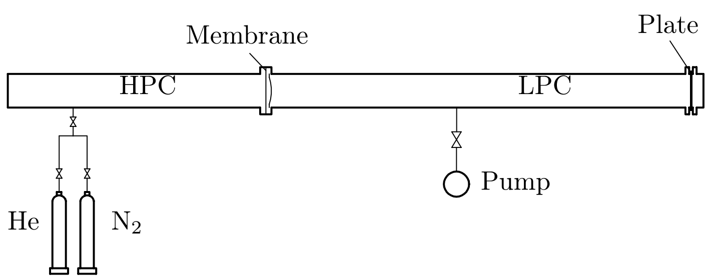

Fig. 1. Principle of the shock tube.

In previous studies, these experiments were conducted to validate structural models and material laws. Material parameters were determined by separate tension tests. All plate and tensile specimens are cut out of the same metal sheets.

This ensures that the material properties hardly vary between experiments with different specimens. This was investigated by repeating the same tension tests several times. All experiments were carried out with the same boundary conditions. In Fig. 2 the middle point displacement of a shock-wave loaded plate is shown together with pressure acting on it with respect to the time. This deformation is simulated with the FEM and the ANN in the following sections.

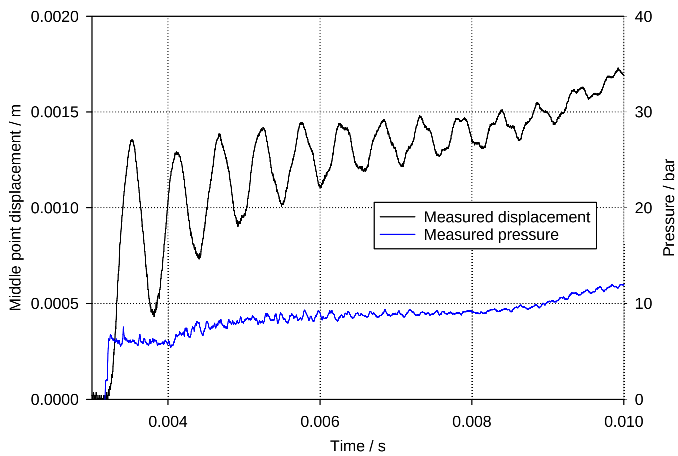

Fig. 2. Measured plate deflection and pressure.

3. Structural model and finite element approach

The structural model used in the present study is based on a layered geometrically nonlinear first-order shear deformation shell theory, which is combined with a physically nonlinear viscoplastic constitutive law. Details about the shell model can be found in [22]. The present study focuses on the finite element implementation versus the new ANN approach.

In the finite element mesh of the plate nine-node isoparametric shell elements are used in an in-house code. The entire displacement field of an element can be expressed by

$$\boldsymbol{v} = \boldsymbol{N}\boldsymbol{q}, \tag{3.1}$$

with $\boldsymbol{N}$ as the matrix of shape functions, which can be found in [23]. The vector $\boldsymbol{q}$ includes all nodal displacements and rotations. The stress resultants in the shell are written as

$$\boldsymbol{R}^T = \begin{bmatrix} \overset{0}{\boldsymbol{N}} & \overset{1}{\boldsymbol{N}} & \overset{2}{\boldsymbol{N}} & \overset{0}{\boldsymbol{Q}} & \overset{1}{\boldsymbol{Q}} \end{bmatrix} \tag{3.2}$$

with

$$\overset{n}{\boldsymbol{N}}{}^T = \left[\begin{array}{ccc} \overset{n}{R}{}^{11} & \overset{n}{R}{}^{22} & \overset{n}{R}{}^{12} \end{array} \right], \quad \overset{n}{\boldsymbol{Q}}{}^T = \left[\begin{array}{cc} \overset{n}{R}{}^{23} & \overset{n}{R}{}^{13} \end{array} \right] \tag{3.3}$$

denoting section forces and moments of orders belonging to the geometrically nonlinear shell theory. Due to the development of strain-displacement relations higher order terms are obtained in strains and generalized forces. The dependency between strain vector and vector of nodal displacements and rotations is expressed by a nonlinear transformation matrix $\boldsymbol{B}$

$$\boldsymbol{\varepsilon} = \left[\begin{array}{ccccc} \overset{0}{\boldsymbol{\varepsilon}} & \overset{1}{\boldsymbol{\varepsilon}} & \overset{2}{\boldsymbol{\varepsilon}} & \overset{0}{\boldsymbol{\gamma}} & \overset{1}{\boldsymbol{\gamma}} \end{array} \right]^T = \tilde{\boldsymbol{B}}(\boldsymbol{v})\boldsymbol{v} = \tilde{\boldsymbol{B}}(\boldsymbol{v})\boldsymbol{N}\boldsymbol{q} = \boldsymbol{B}(\boldsymbol{v})\boldsymbol{q} \tag{3.4}$$

with

$$\overset{n}{\boldsymbol{\varepsilon}}{}^T = \left[\begin{array}{ccc} \overset{n}{\varepsilon}_{11} & \overset{n}{\varepsilon}_{22} & 2\,\overset{n}{\varepsilon}_{12} \end{array} \right], \quad \overset{n}{\boldsymbol{\gamma}}{}^T = \left[\begin{array}{cc} 2\overset{n}{\varepsilon}_{23} & 2\overset{n}{\varepsilon}_{13} \end{array} \right]. \tag{3.5}$$

The matrix $\tilde{\boldsymbol{B}}$ is divided into a linear and nonlinear part $\tilde{\boldsymbol{B}}_{\boldsymbol{L}}$ and $\tilde{\boldsymbol{B}}_{\boldsymbol{NL}}$. The nonlinear term can be represented as the product of two matrices $\boldsymbol{G}$ and $\boldsymbol{A}$ in the form $\tilde{\boldsymbol{B}}_{\boldsymbol{NL}} = \boldsymbol{A}(\boldsymbol{q})\boldsymbol{G}$ where $\boldsymbol{G}$ depends on the element geometry only, and $\boldsymbol{A}$ is a function of the geometry and of the nodal displacements and rotations. The virtual strains are expressed by

$$\delta\boldsymbol{\varepsilon} = \delta(\boldsymbol{B}\boldsymbol{q}) = (\tilde{\boldsymbol{B}}_{\boldsymbol{L}}\boldsymbol{N} + \boldsymbol{A}(\boldsymbol{q})\boldsymbol{G}\boldsymbol{N})\delta\boldsymbol{q} = \bar{\boldsymbol{B}}\delta\boldsymbol{q}. \tag{3.6}$$

Details of the components of the matrices $\tilde{\boldsymbol{B}}_{\boldsymbol{L}}$, $\boldsymbol{A}$, $\boldsymbol{G}$ are reported in [23]. External loads are covered by a vector $\boldsymbol{F}_{(k)}$ for each layer k and surface loads are denoted by $\boldsymbol{p}$. The vector of the resulting forces and moments at the boundary in each layer k is summarized with ${}^*\boldsymbol{L}_{(k)}$. The vector of inertia forces and moments in each layer k can be written as

$$\boldsymbol{I}_{(k)} = \boldsymbol{i}_{(k)}\ddot{\boldsymbol{v}} = \boldsymbol{i}_{(k)}\boldsymbol{N}\ddot{\boldsymbol{q}} \tag{3.7}$$

and analogously the vector of the damping forces is expressed by

$$\boldsymbol{D}_{(k)} = \boldsymbol{d}_{(k)}\dot{\boldsymbol{v}} = \boldsymbol{d}_{(k)}\boldsymbol{N}\dot{\boldsymbol{q}}. \tag{3.8}$$

By means of these quantities the principle of virtual work for the finite element implementation can be written in a discrete form:

$$\int\limits_{\mathcal{M}} \boldsymbol{R}^T \delta \overset{n}{\boldsymbol{\varepsilon}}\, d\mathcal{M} = \delta\boldsymbol{q}^T \int\limits_{\mathcal{M}} \bar{\boldsymbol{B}}^T \boldsymbol{R} d\mathcal{M} = \delta\boldsymbol{q}^T\boldsymbol{Q}, \tag{3.9}$$

$$-\int\limits_{\mathcal{M}}\sum_{k=1}^{\ell}\boldsymbol{F}_{(k)}^{T}\delta\boldsymbol{v}d\mathcal{M}=-\delta\boldsymbol{q}^{T}\int\limits_{\mathcal{M}}\boldsymbol{N}^{T}\boldsymbol{F}d\mathcal{M}=-\delta\boldsymbol{q}^{T}\boldsymbol{R}_{1},\tag{3.10}$$

$$-\delta\boldsymbol{q}^{T}\int\limits_{\mathcal{M}}\boldsymbol{N}^{T}\boldsymbol{p}d\mathcal{M}=-\delta\boldsymbol{q}^{T}\boldsymbol{R}_{2},\tag{3.11}$$

$$-\int\limits_{\mathcal{L}}\sum_{k=1}^{\ell}{}^{*}\boldsymbol{L}_{(k)}^{T}\delta\boldsymbol{v}d\mathcal{L}=-\delta\boldsymbol{q}^{T}\int\limits_{\mathcal{L}}\boldsymbol{N}^{T}\boldsymbol{L}d\mathcal{L}=-\delta\boldsymbol{q}^{T}\boldsymbol{R}_{3},\tag{3.12}$$

$$\begin{aligned}\int\limits_{\mathcal{M}}\sum_{k=1}^{\ell}\boldsymbol{I}_{(k)}^{T}\delta\boldsymbol{v}d\mathcal{M}&=\int\limits_{\mathcal{M}}(\boldsymbol{i}\boldsymbol{N}\ddot{\boldsymbol{q}})^{T}\boldsymbol{N}d\mathcal{M}\delta\boldsymbol{q}=\delta\boldsymbol{q}^{T}\int\limits_{\mathcal{M}}\boldsymbol{N}^{T}\boldsymbol{i}\boldsymbol{N}d\mathcal{M}\ddot{\boldsymbol{q}}\\&=\delta\boldsymbol{q}^{T}\boldsymbol{M}\ddot{\boldsymbol{q}},\end{aligned}\tag{3.13}$$

$$\begin{aligned}\int\limits_{\mathcal{M}}\sum_{k=1}^{\ell}\boldsymbol{D}_{(k)}^{T}\delta\boldsymbol{v}d\mathcal{M}&=\int\limits_{\mathcal{M}}(\boldsymbol{d}\boldsymbol{N}\dot{\boldsymbol{q}})^{T}\boldsymbol{N}d\mathcal{M}\delta\boldsymbol{q}=\delta\boldsymbol{q}^{T}\int\limits_{\mathcal{M}}\boldsymbol{N}^{T}\boldsymbol{d}\boldsymbol{N}d\mathcal{M}\dot{\boldsymbol{q}}\\&=\delta\boldsymbol{q}^{T}\boldsymbol{C}\dot{\boldsymbol{q}}.\end{aligned}\tag{3.14}$$

This leads to the principle of virtual work in the form

$$\delta\boldsymbol{q}^{T}\left(\boldsymbol{Q}-\boldsymbol{R}_{1}-\boldsymbol{R}_{2}-\boldsymbol{R}_{3}+\boldsymbol{M}\ddot{\boldsymbol{q}}+\boldsymbol{C}\dot{\boldsymbol{q}}\right)=0.\tag{3.15}$$

Consequently, the term in brackets leads to the system of equations of motion

$$\boldsymbol{M}\ddot{\boldsymbol{q}}+\boldsymbol{C}\dot{\boldsymbol{q}}+\boldsymbol{Q}=\boldsymbol{R}\tag{3.16}$$

with $\boldsymbol{R}=\boldsymbol{R}_1+\boldsymbol{R}_2+\boldsymbol{R}_3$. For solving this system of differential equations the central difference method is applied. Considering a time increment Δt, this leads for time t to

$$\ddot{\boldsymbol{q}}_{t}=\frac{1}{\Delta t^{2}}\left(\boldsymbol{q}_{t-\Delta t}-2\boldsymbol{q}_{t}+\boldsymbol{q}_{t+\Delta t}\right),\tag{3.17}$$

$$\dot{\boldsymbol{q}}_{t}=\frac{1}{2\Delta t}\left(-\boldsymbol{q}_{t-\Delta t}+\boldsymbol{q}_{t+\Delta t}\right).\tag{3.18}$$

The vector of generalized nodal displacements at time $t+\Delta t$ is then expressed by

$$\boldsymbol{q}_{t+\Delta t}=\frac{\boldsymbol{R}_{t}-\boldsymbol{Q}_{t}-\frac{1}{\Delta t^{2}}\boldsymbol{M}\left(\boldsymbol{q}_{t-\Delta t}-2\boldsymbol{q}_{t}\right)+\frac{1}{2\Delta t}\boldsymbol{C}\boldsymbol{q}_{t-\Delta t}}{\frac{1}{\Delta t^{2}}\boldsymbol{M}+\frac{1}{2\Delta t}\boldsymbol{C}}.\tag{3.19}$$

For the viscoplastic material behaviour the constitutive law of Lemaitre–Chaboche [24] with kinematic hardening is implemented [14]. The plastic strain rate tensor is expressed as

$$\dot{\varepsilon}^p_{ij} = \frac{3}{2}\dot{p}\frac{\sigma^{'}_{ij} - X^{'}_{ij}}{J_2(\sigma^{'}_{rs} - X^{'}_{rs})}, \tag{3.20}$$

$$\dot{p} = \left\langle \frac{\sigma_v}{K} \right\rangle^v, \tag{3.21}$$

$$\sigma_v = J_2(\sigma^{'}_{ij} - X'_{ij}) - k, \tag{3.22}$$

$$\dot{X}_{ij} = \frac{2}{3}a\dot{\varepsilon}^p_{ij} - sX_{ij}\dot{p}. \tag{3.23}$$

Here, ε^p_{ij}, σ_{ij}, X_{ij}, k, p, σ_v denote plastic strain tensor, stress tensor, backstress tensor, yield limit, equivalent plastic strain, overstress, and a, s, v, K are material parameters. The second invariant of a tensor is abbreviated with $J_2()$. The deviatoric part of a tensor is denoted by $()^{'}$, $\dot{()}$ stands for the time derivative. All material parameters are identified by tension tests.
These physically nonlinear constitutive equations are integrated by the trapezoidal rule. Following this approach the increment of the plastic strains and of the hardening parameters at each time step are calculated as:

$$\Delta\boldsymbol{\varepsilon}^p_t = \frac{1}{2}\Delta t\left(\dot{\boldsymbol{\varepsilon}}^p_{t-\Delta t} + \dot{\boldsymbol{\varepsilon}}^{p,i}_t\right), \tag{3.24}$$

$$\Delta\boldsymbol{X}_t = \frac{1}{2}\Delta t\left(\dot{\boldsymbol{X}}_{t-\Delta t} + \dot{\boldsymbol{X}}^i_t\right). \tag{3.25}$$

The current values are obtained by

$$\boldsymbol{\varepsilon}^p_t = \boldsymbol{\varepsilon}^{p,i}_t = \boldsymbol{\varepsilon}^p_{t-\Delta t} + \Delta\boldsymbol{\varepsilon}^p_t, \qquad \boldsymbol{X}_t = \boldsymbol{X}^i_t = \boldsymbol{X}_{t-\Delta t} + \Delta\boldsymbol{X}_t. \tag{3.26}$$

Here, i denotes the number of iterations.

This complex nonlinear system of equations is the basis for the finite element simulations in this study. The calculated results, and especially their sensitivity to changes in material parameters, are compared to results based on the ANN described in the next section.

4. Artificial neural network

In order to replace the above described complex nonlinear structural and material model, an efficient alternative is proposed. Due to the fact, that an artificial neural network is based on a self-learning algorithm, material parameters as in the present finite element study, do not occur. The proposed network learns by experiences from experimental data. From the variety of ANNs, the well-established type of a feed-forward ANN [25] is chosen for the present type of structural deformation. During the training procedure, additional hidden layers

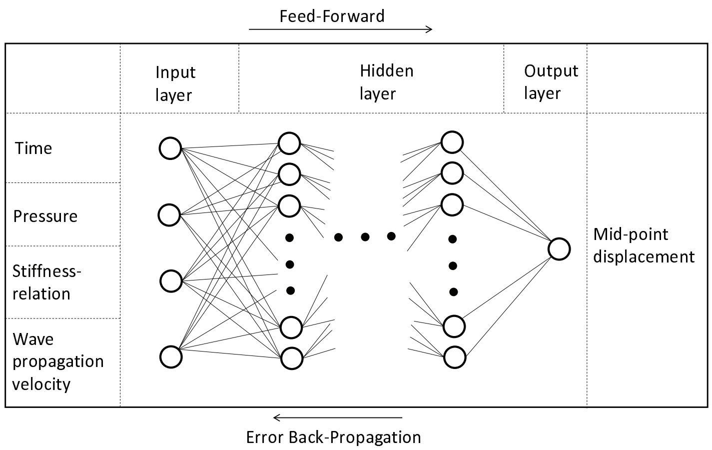

Fig. 3. Feed forward artificial neural network.

are added iteratively by the user and the accuracy is investigated in the following section. Four input variables, such as time, pressure, stiffness relation and wave propagation velocity, are applied. Several different materials can be used for the plate specimen. In order to account in the ANN for this effect, a stiffness relation between the Young's moduli of the used materials is introduced. If only steel material is used as in the following examples, then the third input parameter is constant throughout the training and behaves like a bias. The wave propagation velocity depends on the gas used in the shock tube. This neuron is important in this study to provide unique input data. The wave propagation speed depends on the used gas in the HPC. If different gases are used in two experiments, then two measured pressures at one instance of time could be equal but the plate displacements are different. This is due to different strain rates caused by different wave propagation speeds. In order to keep unique ordered pairs of values, the wave propagation is taken into account. The output layer contains one neuron for the mid-point displacement of the plate. The number of neurons in up to four hidden layers changes between eight and ten, depending on the achieved accuracy during the training procedure. Here, the criterion for an optimal training is the minimised difference between measured and trained mid-point displacement, obtained by the least square method. In Fig. 3, the feed-forward neural network with the gradient descent algorithm for the error back propagation is shown. Normalised values of all variables are introduced due to better convergence [1, 26]. This is carried out for input and output values x_i by

$$X_i = 0.1 + 0.8 \cdot \left(\frac{x_i - x_{min}}{x_{max} - x_{min}} \right) \tag{4.1}$$

leading to unified values X_i and with x_{min} and x_{max} as minimum and maximum values of each input and output value, respectively. The propagation function includes the weights w_{ij}, which have to be determined iteratively in the ANN,

$$p_j = \sum_{i=1}^{n} X_i w_{ij}, \tag{4.2}$$

where n is the number of inputs. In this neural network, the number of hidden layers and neurons in the hidden layers can vary. According to a number of m layers including input and output layers, $(m-1)$ matrices are obtained. In the activation function F_j for one neuron j, the sigmoid function is implemented:

$$F_j = \frac{1}{1+e^{-p_j}}. \tag{4.3}$$

In the training procedure the number of hidden layers is increased in several calculations iteratively by the user in order to avoid overfitting; or in other words, only as many hidden layers are applied as necessary to account for the oscillating output signal. The problem of overfitting is addressed in the next section, where the accuracy of the trained network is studied. Following this method, an additional regularisation method was not necessary. The entire algorithm was implemented in python. As a stopping criterion a maximum number of 600000 epochs is defined in this study. Thereby, convergence was reached in all shown examples. As a criterion for the stability of the ANN predictions the difference between measured and calculated first lower amplitude is introduced. In preliminary studies [14] it was shown that this difference is the most affected value immediately after the shock wave load during the considered viscoplastic vibrations. The simulated upper amplitudes are closer to the measurement as the lower ones. In Table 1 in the following section, these quantities are described.

5. Results and discussion

In Fig. 2, a typical pressure evolution is shown, which occurs on the plate specimen, when the shock wave reaches the plate. Corresponding to this pressure load, the mid-point displacement of the plate is indicated in the diagram.

In Fig. 4, two examples of finite element simulations are presented and are compared to the measured mid-point displacement in 2. Changes in the viscous material properties are indicated in the legend. The calculated results correspond to the measurement, however, a sensitivity especially of the lower amplitudes is observed depending on changes in the material parameters. The differences between the simulated first lower amplitude and the measured one are +5.9% and +34.9% for FE-Simulation 1 and 2, respectively. Details about these sensitivity investigations can be found in [14].

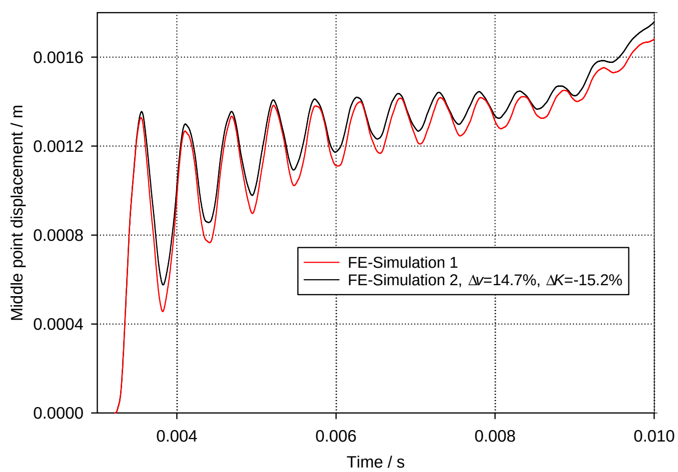

Fig. 4. Simulated plate deflections with material parameter variations.

Due to the fact, that strain rates between $100\mathrm{s}^{-1}$ and $300\mathrm{s}^{-1}$ occur in the shock tube experiments, it is difficult to identify viscous parameters by material testing machines and, hence, scattering of these parameters occurs. Consequently, uncertainties are involved in the finite element simulations, because the viscosity significantly influences the predicted result. For this reason, an alternative approach is chosen with an ANN, which does not need a material law and, hence, does not depend on material parameter variations. However, changes in input parameters can still cause variations in output results.

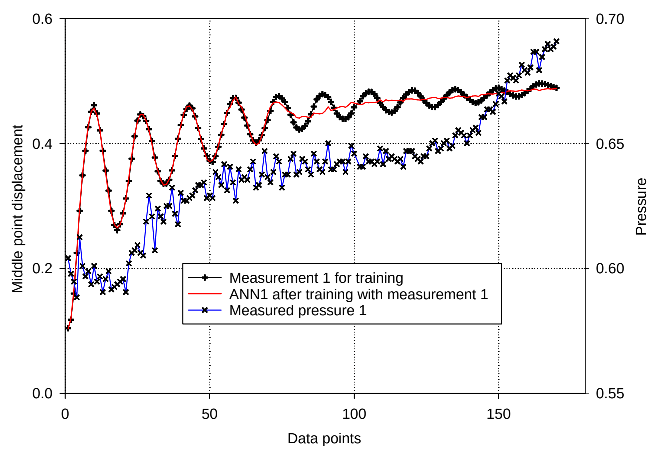

Fig. 5. Measurement and ANN simulation.

In Fig. 5, the measured mid-point deflection and the pressure, which is also presented in Fig. 2, is shown in normalised form with respect to the number of data points. Here, 170 data points, consisting of 170 values for each time, pressure, stiffness, and velocity are used for each measurement and calculation. Equivalently 170 mid-point displacement values are used for the output neuron. The graphs are plotted continuously over the number of data points. The time increment between two values is $3.4 \cdot 10^{-5}s$, which is small compared to a period of oscillation in Fig. 2.

In Fig. 6 it is investigated how many hidden layers can be used to increase the accuracy of the trained network. As indicated in the legend, it was determined by means of the RMSE, that three hidden layers lead to the most accurate results.

In order to introduce scattering of input values, an additional shock tube experiment with similar pressure evolution is carried out and shown in Fig. 7.

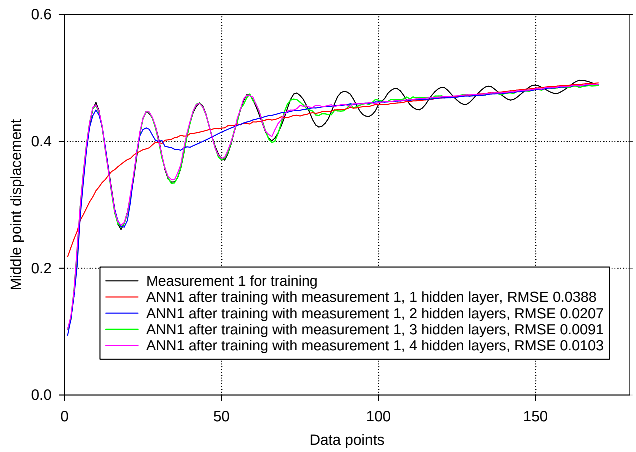

Fig. 6. Measurement and ANN simulation with different number of hidden layers.

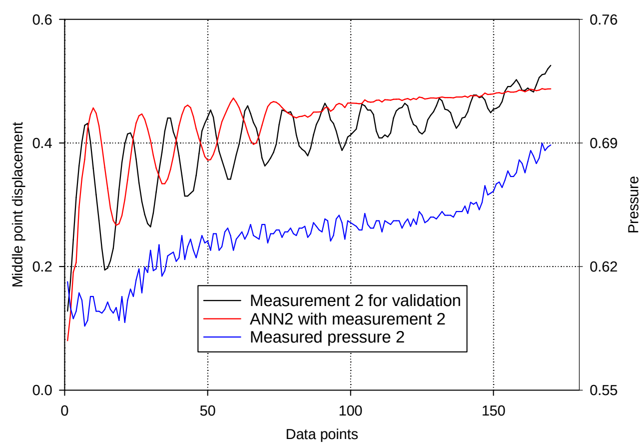

Fig. 7. Measurement and ANN simulations with input parameter variation.

The measured mid-point deflection changes due to small pressure variations. Consequently, it is investigated which variation in the calculated results by means of the ANN occurs. Firstly, the ANN is trained with measurement 1 in Fig. 5. The pressure evolution from Fig. 4 is normalised and shown in Fig. 5 for this purpose. As a result, the ANN predicts nearly identical the measurement from 1 until to 70 data points. After these data points, the ANN calculates an average between the amplitudes. Secondly, a varied pressure evolution (measured pressure 2), see Fig. 7, corresponding to measurement 2 is inserted into the already trained ANN, expecting a prediction of its mid-point displacement. But the result is nearly the same mid-point deflection as for the measurement 1, which is shown in Fig. 7.

Table 1. Variation of first lower amplitudes in ANN predictions.

Measure-ment	ANN1	ANN2 $\Delta p_{max} = +1.8\%$	ANN3	ANN4 $\Delta p_{max} = -9.5\%$	ANN5 $\Delta p_{max} = 30.5\%$	ANN5 $\Delta p_{max} = 14.5\%$
1	**+1.5%**	**+2.2%**			∅	**-10.3%**
2		+37.2%				
3			**-1.5%**	**+5.4%**	∅	∅
4				+22.2%		

Obviously, the once trained network behaves very stable with respect to variations in input parameters. The defined criterion for quantifying the stability of the ANN calculation is the difference between measured and calculated first lower amplitude, which is indicated in Table 1. The pressure difference until to the first lower amplitude in the two ANN predictions ANN1 and ANN2 in Figs. 5, 7 is $\Delta p_{max} = +1.8\%$. The difference of the first lower amplitude between measured displacement and calculated displacement by means of the training with ANN1 is only $+1.5\%$. The trained network predicts the measurement 1 even stable, if the measured pressure 2 is used as input. This turns out in the difference of 2.2% between the measured and predicted first lower amplitude with ANN2. This reveals the stability of the trained network. Compared to the measurement 2 the difference is 37.2%. The stable results in Table 1 are marked in bold, also for the next example.

As mentioned in the introduction, in the literature, the effect is often described that ANN predictions can be uncertain, since input data is used which differs from the trained data set. In the present study, it can be confirmed that input data, which does not match the trained data, does not lead to the measured output data. However, in the present study, the ANN simulation leads to the trained output even if input data changes. This phenomenon makes the ANN model very accurate und insensitive to changes in input parameters. All ANN calculations in Fig. 5, 7 were carried out with three hidden layers and eight neurons in each layer.

In Figs. 8, 9 two additional experiments and ANN predictions with a steel plate are presented. Here, four hidden layers with 10 neurons in each layer are applied to obtain the accuracy between the measurement 3 and the trained ANN as shown in Fig. 8. Due to the indicated different pressure evolutions (measured pressures 3 and 4) the mid-point displacement of the measurement 4 is different from the measurement 3 in the experiments. However, if pressure 4 is inserted in the trained ANN, nearly the same mid-point displacement is obtained as with measured pressure 3. Again, the trained ANN behaves very insensitive to changes in their input parameters.

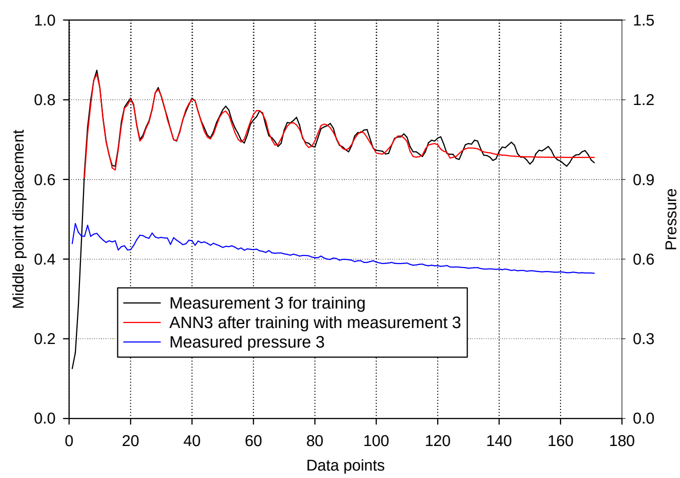

Fig. 8. Additional measurement and ANN simulation.

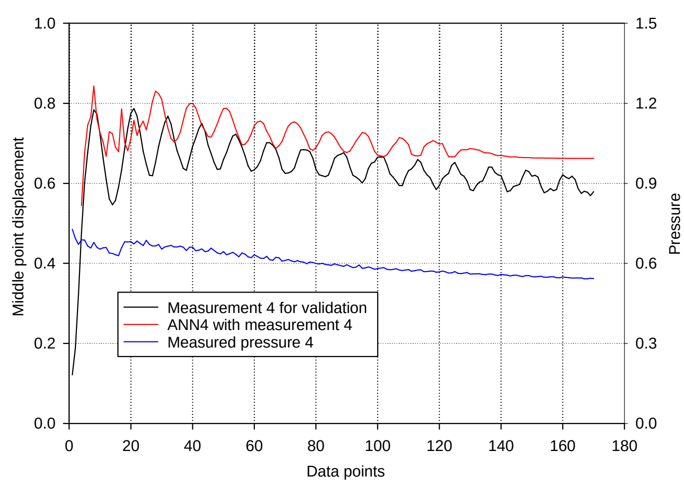

Fig. 9. Additional measurement and ANN simulation with input parameter variation.

In Table 1, the differences of the measured pressures 3 and 4 ($\Delta p_{max} = -9.5\%$) together with the deviations of the first lower amplitudes are shown. The trained network has only a slight difference of -1.5% to the measured displacement 3. If the measured pressure 4 is inserted in this trained ANN a difference of $+5.4\%$ is obtained, which again confirms the stable simulation of the measurement 3 even if differences in the input pressure occurs. The difference of ANN4 to the measurement 4 is $+22.2\%$.

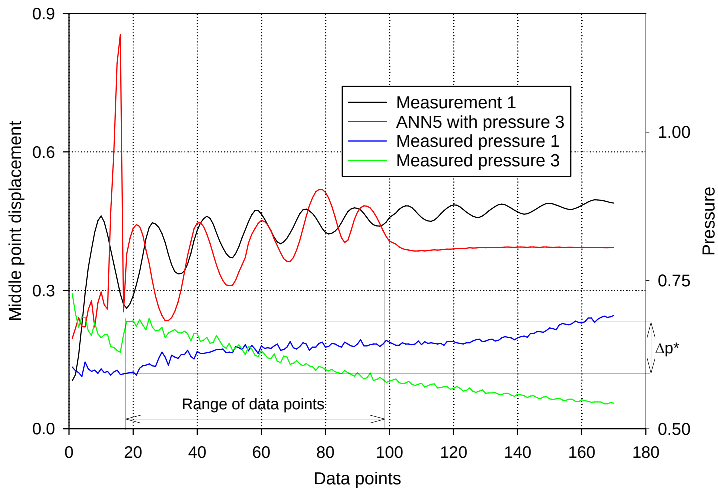

Fig. 10. Study of range of input data for stable ANN simulations.

In order to search for the limits of the stability of the trained ANN, in Fig. 10 an example with extreme different pressure evolutions is given. The measured mid-point displacement 1 and pressure 1 from Fig. 5 is shown in the diagram. Additionally, the displacement and pressure of the measurement 3 from Fig. 8 are used here. The measured pressure 3 is inserted into the already trained network (with the measurement 1), which physically does not belong to the training data. However, the ANN tries to force a correlation with the trained mid-point displacement (see ANN with the measurement 3). At the beginning of the calculation until 20 data points, the ANN predicts a displacement similar to the measurement 3. Then this prediction changes suddenly to a displacement similar to the trained data of the ANN, and finally, the calculation differs from the trained data after 100 data points. It seems that the ANN calculation tends towards its trained data since the input data remains in a special range, which is similar to the once trained data set. In the present example, this would be the pressure range Δp^* indicated in Fig. 10. In this range, the difference of the input data is small enough to predict the output data of the trained data set. This observation is also visible in Table 1. During a large pressure difference between the measured pressure 3 and 4 at the beginning of the shock wave load of 30.5% the measured displacement 1 is not predicted with ANN5 at all (empty set in Table 1). After the pressure difference decreased down to 14.5% the measured displacement 1 is calculated with a difference in the first lower amplitude of −10.3%. That means, even though the pressure 3 physically does not belong to the measurement 1, the simulation ANN5 calculates the measured displacement with round about 10% difference. Again the trained network behaves stable in that sense.

6. Conclusions

In the present study about shock-wave loaded structures, it was shown that an ANN can behave very accurately and stable even if variations in input parameters occur. This observation reveals ANN predictions in a different light. A once trained ANN is not used for predicting structural deformations with additional loading data, but it was shown that the trained ANN behaves very stable, if input parameters change. Even if the input data is beyond a physical admissible scattering, the ANN tends to the once trained output data. This makes the simulation of structural deformation accurate. However, this works only inside certain ranges of input values, which can be the contents of further studies. Uncertainties, as they are observed in finite element simulations due to material parameter variations, do not occur, since the ANN works without any material data. Moreover, it was possible to replace a geometrically and physically nonlinear structural model by an artificial neural network.

References

1. M. Shakiba, N. Parson, X.G. Chen, *Modeling the effects of Cu content and deformation variables on the hight-temperature flow behavior of dilute Al-Fe-Si alloys using an artificial neural network*, Materials, **9**, 536, 1–13, 2016.

2. A.-A. Chojaczyk, A.P. Teixeira, C. Luìs, J.-B. Cardosa, C.-G. Soares, *Review and application of artificial neural networks models in reliability analysis of steel structures*, Structural Safety, **52**, A, 78–89, 2015.

3. D. Zhao, D. Ren, K. Zhao, S. Pan, X. Guo, *Effect of welding parameters on tensile strength of ultrasonic spot welded joints of aluminum to steel by experimentation and artificial neural network*, Journal Manufacturing Processes, **30**, 63–74, 2017.

4. J. Cheng, Q.S. Li, *Reliability analysis of structures using artificial neural network based genetic algorithms*, Computer Methods in Applied Mechanics and Engineering, **197**, 3742–3750, 2008.

5. J. Mathew, D. Parfitt, K. Wilford, N. Riddle, M. Alamaniotis, A. Chroneos, M. E. Fitzpatrick, *Reactor pressure vessel embrittlement: Insights from neural network modelling*, Journal of Nuclear Materials, **502**, 311–322, 2018.

6. S. Mandal, P.V. Sivaprasad, S. Venugopal, K.-P.-N. Murthy, *Artificial neural network modeling to evaluate and predict the deformation behavior of stainless steel type AISI 304L during hot torsion*, Applied Soft Computing, **9**, 237–244, 2009.

7. A.A. Javadi, T.P. Tan, M. Zhang, *Neural network for constitutive modelling in finite element analysis*, Computer Assisted Mechanics and Engineering Sciences, **10**, 4, 523–529, 2003.

8. M. Lefik, D.-P. Boso, B.A. Schrefler, *Artificial neural networks in numerical modeling of composites*, Computer Methods in Applied Mechanics and Engineering, **198**, 1785–1804, 2009.

9. T. Chen, H. Chen, *Universal approximation to non-linear operators by neural networks with arbitrary activation functions and its application to dynamical systems*, IEEE Transactions on Neural Networks, **6**, 4, 911–917, 1995.

10. A. Ajmani, D. Kamthania, M.N. Hoda, *A Comparative Study on Constructive and Non- Constructive Supervised Learning Algorithms For Artificial Neural Networks*, Proceedings of the 2nd National Conference, Bharati Vidyapeeths Institute of Computer Applications and Management, INDIACom, New Delhi, 2008.

11. R. Kaunda, *New artificial neural networks for true triaxial stress state analysis and demonstration of intermediate principal stress effects on intact rock strength*, Journal of Rock Mechanics and Geotechnical Engineering, **6**, 338–347, 2014.

12. A.A. Javadi, M. Rezania, *Applications of artificial intelligence and data mining techniques in soil modeling*, Geomechanics and Engineering, **1**, 1, 53–74, 2009.

13. M. Lu, S.-M. AbouRizk, U.H. Hermann, *Sensitivity analysis of neural networks in spool fabrication productivity studies*, Journal of Computing in Civil Engineering, **15**, 4, 299–308, 2001.

14. M. Stoffel, *Sensitivity of simulations depending on material parameter variations*, Mechanics Research Communications, **32**, 332–336, 2005.

15. T.A. Bui, H. Wong, F. Deleruyelle, L.Z. Xie, D.T. Tran, *A thermodynamically consistent model accouting for viscoplastic creep and anisotropic damage in unsaturated rocks*, International Journal of Solids and Structures, **117**, 26–38, 2017.

16. F.C. Salvado, F. Teixeira-Dias, S.M. Walley, L.J. Lea, J.B. Cardoso, *A review on the strain rate dependency of the dynamic viscoplastic response of FCC metals*, Progress in Materials Science, **88**, 186–231, 2017.

17. A.-A. Javadi, M. Rezania, *Intelligent finite element method: An evolutionary approach to constitutive modeling*, Advanced Engineering Informatics, **23**, 442–451, 2009.

18. M.H. Shojaeefard, M. Akbari, M. Tahani, F. Farhani, *Sensitivity analysis of the artificial neural network outputs in friction stir lap joining of aluminium to brass*, Advances in Materials Science and Engineering, **2013**, ID 574914, 1–7, 2013.

19. M. Stoffel, F. Bamer, B. Markert, *Artificial neural networks and intelligent finite elements in non-linear structural mechanics*, Thin-Walled Structures, **131**, 102–106, 2018.

20. M. Stoffel, F. Bamer, B. Markert, *Neural network based constitutive modeling of nonlinear viscoplastic structural response*, Mechanics Research Communications, **95**, 85–88, 2019.

21. J. Schmidhuber, *Deep learning in neural networks: An overview*, Neural Networks, **61**, 85–117, 2015.

22. M. Stoffel, R. Schmidt, D. Weichert, *Shock wave-loaded plates*, International Journal of Solids and Structures, **38**, 7659–7680, 2001.

23. M. Stoffel, R. Schmidt, D. Weichert, *Numerical and Experimental Analysis of Shock Wave-loaded Plates*, Mechanik Berichte Nr. 3, Institute of General Mechanics, RWTH Aachen University, Aachen, 2001.

24. J. Lemaitre, J.L. Chaboche, *Mechanics of Solid Materials*, Cambridge University Press, Cambridge, 1994.

25. V.-K. Ojha, A. Abraham, V. Snášel, *Metaheuristic design of feedforward naural networks: A review of two decades of research*, Engineering Applications of Artificial Intelligence, **60**, 97–116, 2017.

26. Z. Lu, Q. Pan, X. Liu, Y. Qin, Y. He, S. Cao, *Artificial neural network prediction to the hot compressive deformation behavior of Al-Cu-Mg-Ag heat-resistant aluminium alloy*, Mechanics Research Communications, **38**, 192–197, 2011.

Received October 26, 2018; revised version January 30, 2019.
Published online April 30, 2019.